Nonlocal Electronic Distribution in Metallic Clusters: A Critical Examination of Aromatic Stabilization

AYAN DATTA, SAIRAM S. MALLAJOSYULA, AND SWAPAN K. PATI*

Theoretical Sciences Unit, Chemistry and Physics of Materials Unit and DST Unit on Nanoscience, Jawaharlal Nehru Centre for Advanced Scientific Research, Jakkur Campus, Bangalore 560 064, India

Received September 8, 2006

ABSTRACT

All-metal clusters, such as Al_4M_4 (M = alkali metal ion), exhibit interesting features of multi-fold aromaticity/antiaromaticity. Such characteristics arise particularly because of the poor $\sigma-\pi$ separation in this class of systems. This Account presents computational strategies to unambiguously determine the aromaticity/antiaromaticity characteristics of such clusters. Computations of the linear and nonlinear optical responses show that all-metal clusters are orders of magnitude more polarized than the conventional π-conjugated molecules. We also propose new strategies to stabilize all-metal antiaromatic systems through complexation to transition metals and discuss mechanisms for substitution reactions within the conventional organometallic systems by Al_4M_4. Additionally, we find that these all-metal clusters form stacked superclusters that are extremely stable and aromatic.

1. Introduction

One of the major emerging directions of research in both basic and industrial areas has been to understand the behavior of systems at the nanoscale.[1] Materials at nanoscales are expected to show major differences in various properties compared to their bulk mode counterparts. For example, the surface/volume ratios for the nanoparticles are much larger than those in the bulk. This has resulted in many industrial applications of nanoparticles, such as in catalysis,[2] and also in the application of surface-enhanced Raman scattering.[3]

In search for new nanomaterials, the past decade has witnessed major excitement in the area of all-metal clusters. Boldyrev and Wang, on the basis of their combined theoretical and experimental efforts, have reported the first examples of aromatic all-metal clusters, such as $LiAl_4^-$, $NaAl_4^-$, and $CuAl_4^-$.[4] Such molecules share the structures and properties similar to that for the π-conjugated organics. From molecular orbital analysis and the π-electron count in these systems, the neutral analogues of Al_4^{2-}, such as Na_2Al_4, are found to show large resonance stabilization energy and large diamagnetic ring currents, indicating that they are indeed aromatic. Similar examples of such all-metal aromatic clusters have now been reported for Ga_4^{2-}, In_4^{2-}, and also for mixed systems, such as MAl_3^- (M = Si, Ge, Sn, and Pb) and NaX_3 (X = B, Al, and Ga).[5,6] Recent developments in aromaticity/antiaromaticity of new metal clusters have been reviewed by Boldyrev and Wang[7] and also by Tsipis.[8]

The first example of all-metal antiaromatic molecules, Al_4Li_4 and $Al_4Li_3^-$, was proposed recently by Boldyrev and Wang.[9] Just like its organic antiaromatic counterpart, cyclobutadiene (C_4H_4), the Al_4^{4-} skeleton has a finite bond-length alternation (BLA) between the two consecutive Al−Al bonds and has four π electrons in its frontier orbitals. However, unlike its organic counterpart, Al_4Li_4 possesses a very poor $\sigma-\pi$ separation, resulting in a substantial intermixing of the σ and π orbitals. Furthermore, the frontier orbitals do not have pure π characteristics. On the basis of this fact and nucleus-independent chemical shifts (NICS), Schleyer and co-workers suggested that Al_4Li_4 is actually net σ-aromatic, with the σ-aromatic contribution exceeding the π antiaromaticity.[10,11] Santos and co-workers performed topological analysis on Al_4Li_4 based on electron-localization function (ELF) analysis, and their conclusions were similar to Boldyrev and Wang in that the molecule is net antiaromatic.[12] Sundholm and co-workers have calculated the magnetically induced current densities on Al_4^{4-}, wherein they found it to be nonaromatic.[13] Thus, the exact nature of delocalization of electrons in Al_4Li_4 has been quite controversial.[14]

In this Account, we critically examine the $\sigma-\pi$ separation in these all-metal aromatic and antiaromatic systems and provide a computational tool for measuring the propensity of distortions in any given molecular system even for cases where the $\sigma-\pi$ separation is poor.[15] The all-metal molecules are also considered for their second hyperpolarizability responses.[16] Computational strategies are provided for the stabilization of all-metal antiaromatic systems through coordination to low-valent transition-

Ayan Datta received his undergraduate education at the Calcutta University, West Bengal, India, and completed his Ph.D. in 2006 working under the supervision of Prof. Swapan K. Pati on theoretical chemistry. His research interests include quantum chemistry and statistical mechanics for applications in nonlinear optical responses of molecules and extended systems, stability of nanoclusters, magnetism at all length scales, and electron- and proton-transfer processes in the interface of physics, chemistry, and biology. He is also greatly interested in designing toolkits and softwares for chemical education.

Sairam S. Mallajosyula completed his B.Sc. (honors) in chemistry from the Sri Sathya Sai Institute of Higher Learning, Puttaparthi, India, in 2002. He earned his M.Sc. degree in chemistry from the same university in 2004. He joined JNCASR in 2004 as a junior research fellow. His research involves the theoretical modeling of biomaterials.

Swapan K. Pati obtained his Ph.D. from the Indian Institute of Science, Bangalore, India (1998), followed by postdoctoral work in the department of physics at the University of California—Davis, Davis, CA, and in the chemistry department at Northwestern University, Evanston, IL. He is currently an associate professor at the Jawaharlal Nehru Centre for Advanced Scientific Research, Bangalore, India, and is a junior associate of the Abdus Salam International Centre for Theoretical Physics, Italy. He has been a visiting faculty at Purdue University, University of Tokyo, and the Max Planck Institute for Physics of Complex Systems, Dresden, Germany, to name a few. He is a recipient of the bronze medal from the Material Research Society of India and the Chemical Research Society of India. His research interests include quantum many-body theory, molecular electronics, nonlinear optical phenomena, quantum magnetism, and generalized charge-transfer mechanisms.

* To whom correspondence should be addressed. E-mail: pati@jncasr.ac.in.

10.1021/ar0682738 CCC: $37.00
Published on Web 01/03/2007

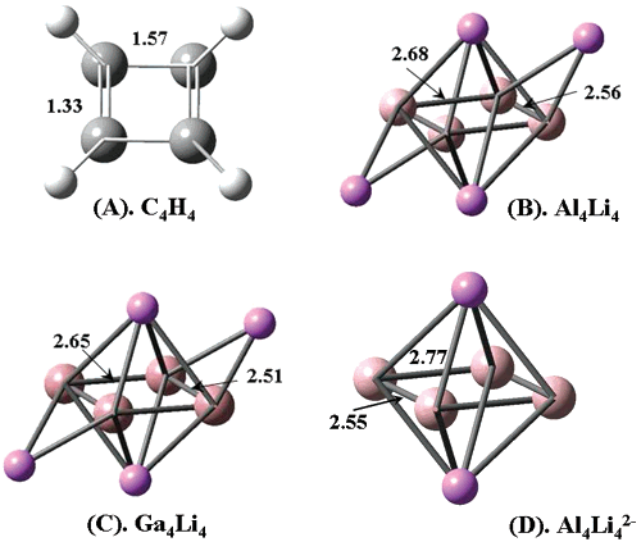

FIGURE 1. GS optimized structure of (A) C_4H_4, (B) Al_4Li_4, (C) Ga_4Li_4, and (D) $Al_4Li_2^{2-}$.

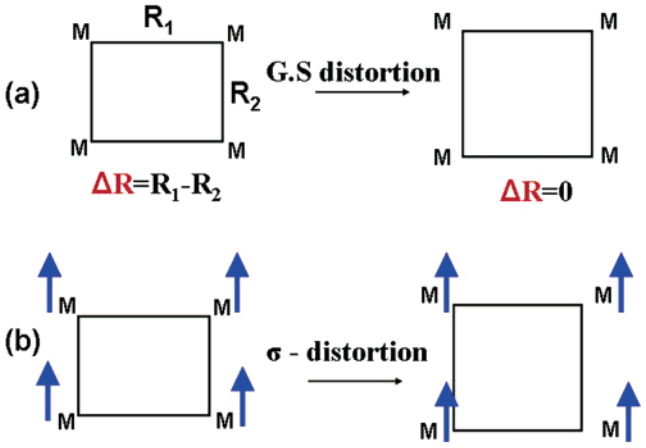

FIGURE 2. (a) Distortion mode for the M_4 rings (M = C, Al, and Ga) in the GS. Li atoms are not shown for the sake of clarity. (b) Distortion in the σ electrons involving the distortion in a high-spin configuration.

metal centers.[17] Reaction pathways are also studied for substitution reactions of C_4H_4 by Al_4M_4 in organometallic systems.[18] Additionally, we find that these all-metal clusters form compact superclusters upon dimerization, which are stable and aromatic.[19]

2. A Model for Quantitative Estimation of $\sigma-\pi$ Distortions in All-Metal Clusters

A very accurate estimation of the nature of σ and π delocalizations can be obtained through a direct $\sigma-\pi$ separation of the energies along the distortion coordinates of the molecular system. Theoretical advancements in such methods have been reviewed earlier.[20,21] The basic idea is to distort the molecules both in the ground-state (GS) geometry and in their highest spin (HS) state by freezing the π electrons in a parallel orientation. The distortion in the HS state thus exclusively involves the σ electrons. Similarly, if one distorts the GS, one derives the contributions from both the σ and π distortions. Subtraction of the distortion energies of the GS and the HS state thus provides an estimate of the π-distortion energies.

To demonstrate the superiority of such a method, we consider a variety of molecular systems: Al_4Li_4, $Al_4Li_4^{2-}$, and Ga_4Li_4. We compare these systems with C_4H_4 and similar organic analogues at each step of $\sigma-\pi$ analysis. These systems have either four or six π electrons in their frontier orbitals and provide a diverse set for unifying the concept of aromaticity or antiaromaticity.

All of the molecular geometries were optimized at the B3LYP/6-311G++ (d,p) level within the Gaussian 03 package.[22] The structures are shown in Figure 1. The GS geometry for both Al_4Li_4 and Ga_4Li_4 has a planar rectangular structure for the ring, with the Li ions occupying positions to maintain a C_{2h} architecture. The BLAs for Al_4Li_4 and Ga_4Li_4 are 0.12 and 0.16 Å, respectively. Note that the same BLA for C_4H_4 is 0.24 Å. The smaller BLA in Al_4/Ga_4 is due to the coordination of two Li atoms with the two short M−M bonds. To verify this, we consider $Al_4Li_2^{2-}$ (Figure 1D), which upon optimization leads to a BLA of 0.22 Å, comparable to C_4H_4. The BLA picture thus suggests a propensity to distort for these all-metal clusters.

The geometry-optimized structures are distorted by ΔR (where ΔR is the difference between the long M−M and short M−M bonds in the M_4 ring), so that the distortion keeps the sum of two adjacent M−M bonds constant (scheme a in Figure 2). The energy associated with the distortion is partitioned into σ and π components as $\Delta E_\pi = \Delta E_{GS} - \Delta E_\sigma$. The σ backbone for a M_4 ring with four π electrons can be modeled as M_4^{4-} with a HS configuration ($S = 2$), where all of the four π electrons are parallel (scheme b in Figure 2). For the six π-electron $Al_4Li_4^{2-}$, however, there are only four π orbitals, and thus, a HS configuration with $S = 3$ is not feasible; rather two parallel spins with $S = 1$ state in $Al_4Li_4^{2-}$ correspond to the HS state. ΔE_{HS} is thus defined as ΔE_π. For the HS systems, UB3LYP calculations are performed at the same basis set level with annihilation of the first spin contaminant.

In Figure 3, the σ and π energies as a function of the distortion parameter, ΔR, are plotted. We have performed an analysis of the fragmentation of the total energy into contributions from the nuclear−nuclear (V_{nn}), electron−nuclear (V_{en}), electron−electron (V_{ee}), and kinetic energy (KE) as a function of BLA. In the inset, the core energy, V_{core} [sum of the kinetic energy and nuclear−electron (ne) interactions], V_{ee}, and V_{nn} are plotted. For all of the systems, it is found that the π electrons have a general tendency of forming a distorted structure (π energy is most stable at large ΔR), while the σ framework opposes the distortion and tends to equalize the bonds. The final structure and thus the propensity to distort or equalize the M−M bond lengths will crucially depend upon the predomination of either of the forces. In Figure 3a, the result for the well-known C_4H_4 system is shown. In this case, the instability associated with the σ-backbone distortion is very little (4 kcal/mol for $\Delta R = 0.1$), while the stability for π distortion is quite substantial (22 kcal/mol for $\Delta R = 0.1$), clearly overwhelming the tendency for σ-backbone equalization. Thus, the C_4H_4 has a rectangular structure with a minor component from σ-backbone

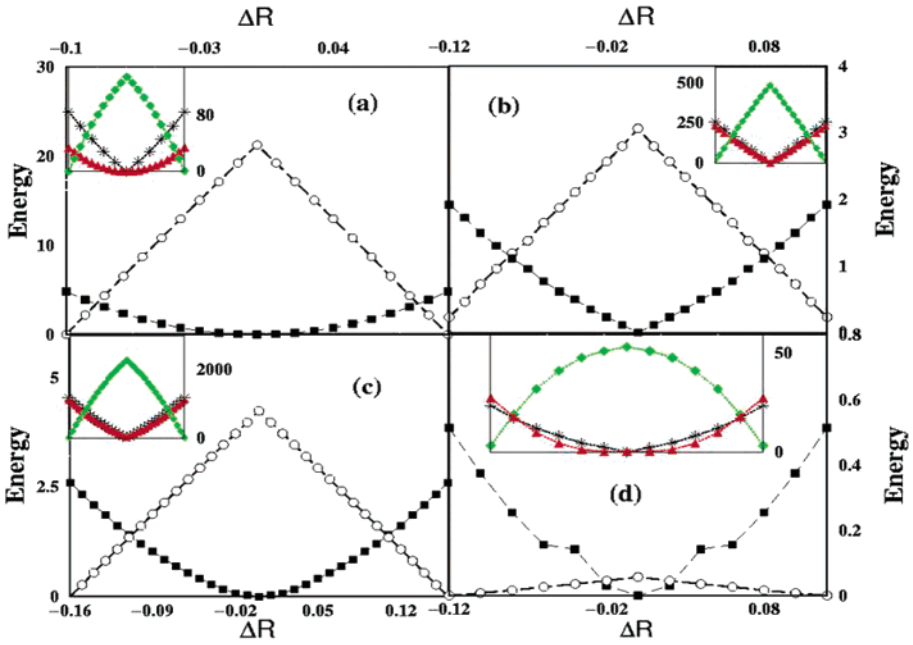

FIGURE 3. Variation of the σ energy (■) and π energy (○), both in kcal/mol, as a function of the distortion axis, ΔR, for (a) C_4H_4, (b) Al_4Li_4, (c) Ga_4Li_4, and (d) $Al_4Li_4^{2-}$. The insets show V_{core} (green), V_{ee} (black), and V_{nn} (red) components in the GS structures. All of the energies are scaled to make the most stable geometry zero in energy, and positive values in the energy axis correspond to destabilization.

equalization. Both V_{ee} and V_{nn} are destabilized with distortion, while the V_{core} component is stabilized. Further analysis shows that it is the V_{ne} term in the V_{core} that favors the distorted structure. This is easy to understand because the V_{ne} component is associated with the electron−lattice interactions and lead to Jahn−Teller stabilization in the distorted structure. However, components, such as V_{ee} and V_{nn}, stabilize the $\Delta R = 0$ structure associated with the delocalized π electrons (for nonzero ΔR, the electron density is localized in shorter bonds). Thus, the actual preference for the highly symmetric or the distorted structure is governed by the competition between all other components and V_{en}. For systems that adapt to a highly symmetric structure ($\Delta R = 0$), V_{en} is only a minor component.

For the all-metal system, however, the $\sigma-\pi$ separation energy plays a crucial role. For example, in Al_4Li_4, the distortion in the σ framework leads to a destabilization of 2.5 kcal/mol, while the π framework gains energy of 3.5 kcal/mol (Figure 3b). The GS energy is thus stabilized by the distortion along the ring. Accordingly, Al_4Li_4 can be labeled as π-distorted, although the propensity of σ-backbone equalization is quite substantial. The energy components also follow very similar trends, such as that for C_4H_4 (inset of Figure 3b). A similar conclusion is also derived for the Ga_4Li_4, where the π stabilization associated with the distortion is 4 kcal/mol, while σ destabilization is 2.5 kcal/mol (as seen in Figure 3c). The π-distorted structure is thus stabilized by an amount of 1.5 kcal/mol, 0.5 kcal/mol more than that for Al_4Li_4. Thus, the π-distortion propensity follows the order: $C_4H_4 > Ga_4Li_4 > Al_4Li_4$.

The fact that this simple $\sigma-\pi$ separation gives a very clear picture for the nature of equalized/distorted M−M bond lengths is evident from Figure 3d, where we have analyzed the case for $Al_4Li_4^{2-}$. Contrary to the previous cases, in $Al_4Li_4^{2-}$, the stabilization associated with the equalization of the σ backbone overwhelms the instability because of π-electron localization by 0.5 kcal/mol and forces the system to be nondistorted. This is of course true for C_6H_6, where σ delocalization exceeds π localization.[21]

3. Charge Transfer Induced Large Linear and Nonlinear Optical Properties of Small Al Clusters: Al_4M_4 (M = Li and Na)

The development of materials with large nonlinear optical (NLO) properties is a key to controlling the propagation of light by optical means. In particular, the response of the materials to the application of the electric field has found tremendous applications in designing materials from application lasers to optical switches and optoelectronics.[23] The NLO properties of organic π-conjugated materials have been studied in great detail in the last 2 decades.[24,25]

While organic π-conjugated systems are stabilized because of π-electron delocalizations, the inorganic metal complexes reduce their energy through strong charge transfer. We have performed the calculations on Al_4Li_4 and Al_4Na_4. The linear and nonlinear optical coefficients are calculated by Zerner's INDO method with multireference double CI (MRDCI) calculations,[26,27] with four reference determinants, including the Hartree−Fock GS, at an electrical frequency of 0.001 atomic unit (au), much below any optical resonance. To directly compare the efficiency of these Al_4 clusters with the conventional π-conjugated systems, the optical properties of the 1,3-cyclobutadiene (C_4H_4) and benzene (C_6H_6) are also calculated at the same level of theory. The optical gaps for Al_4Li_4 and Al_4Na_4 are 0.024 and 0.028 au, while the gaps for C_4H_4 and C_6H_6 are 0.2410 and 0.2588 au, respectively. It is evident that, for

Table 1. GS Dipole Moment, μ_G, Linear Polarizability, α, First Hyperpolarizability, β, and Second Hyperpolarizability, γ (Isotropic Average), for the Molecules from ZINDO−MRDCI Calculations[a]

molecule	μ_G	$\bar{\alpha}$	$\bar{\beta}$	$\bar{\gamma}$
Al_4Li_4	0.00	5.5×10^3	0.00	5.33×10^8
Al_4Na_4	0.00	8.7×10^3	0.00	2.00×10^8
C_4H_4	0.00	2.9×10^2	0.00	4.76×10^3
C_6H_6	0.00	5.4×10^2	0.00	8.44×10^3

[a] The units are in atomic units (au).

the Al_4 clusters, the ΔR is very small compared to the C_4H_4 (antiaromatic, $\Delta R = 0.245$ Å) but larger than C_6H_6 (aromatic, $\Delta R = 0$). For the Al_4 clusters, there is a substantial amount of charge transfer from the alkali atoms to the Al atoms (negative charge), making them act as a donor and an acceptor, respectively. Such a charge transfer induces polarization in the GS structure and reduces the optical gap. On the other hand, with the C−H bond being perfectly covalent, there is almost no charge transfer in the case of C_4H_4 and C_6H_6, and thus, they have a large optical gap because of finite size molecular architecture.

In Table 1, the magnitudes of the GS dipole moment, μ_G, and the linear (α) and nonlinear (β and γ) polarizabilities for the clusters are reported from the ZINDO calculations. Note that the magnitudes for the tumbling averaged $\bar{\alpha}$, $\bar{\beta}$, and $\bar{\gamma}$ are reported, which are defined in terms of their tensor components as

$$\bar{\alpha} = \frac{1}{3}\sum_i (\alpha_{ii}) \quad \bar{\beta} = \sqrt{\sum_i \beta_i \beta^*_i} \quad \beta_i = \frac{1}{3}\sum_j (\beta_{ijj} + \beta_{jij} + \beta_{jji})$$

$$\bar{\gamma} = \frac{1}{15}\sum_{ij} (2\gamma_{iijj} + \gamma_{ijji}) \quad (1)$$

where the sums are over the coordinates x, y, and z ($i, j = x, y, z$) and β^*_i refers to the conjugate of the β_i vector.

The optically active states are the low-energy states of these metallic clusters. Because the optical coefficients are inversely proportional to the optical gaps and proportional to the dipolar matrices, a large optical gap implies low magnitudes for the optical coefficients. C_4H_4 has the highest magnitude of BLA and optical gap and the least charge transfer on the ring structure, thereby the smallest magnitude of $\bar{\gamma}$. On the other hand, although BLA is 0 for C_6H_6, because of complete π-electron delocalization, there is no charge transfer in the finite molecular structure, leading to a large optical gap and weak polarization. Consequently, $\bar{\gamma}$ is also very small for C_6H_6. In contrast, the optical coefficients in general are quite large for the Al_4 clusters. For example, $\bar{\gamma}$ values for the Al_4 clusters are 10^4 times greater than that for C_4H_4 and C_6H_6.[16]

4. Stabilization of the All-Metal Antiaromatic Molecule through Complexation to Transition Metals

From the discussion in the previous section, it is clear that the all-metal charge-transfer clusters are excellent materials for recording a large third harmonic generation. However, these Al_4M_4 compounds being antiaromatic are difficult to synthesize. In fact, the synthesis of antiaromatic molecules is difficult because of their instabilities. Cyclobutadiene (C_4H_4), a four π electron system, remained non-isolated for a long time before Longuet-Higgins and Orgel proposed the concept of stabilization through complexation with a transition metal to form an organometallic compound.[28] In the following section, such a simplistic model is justified for the small Al_4 clusters and we propose a few very stable complexes for these all-metal species. Parallelly, these compounds are compared and contrasted with their organic analogues (C_4H_4 complexes).

A simple Hückel π-electron theory predicts a triplet square geometry for C_4H_4 with equal C−C bond lengths.[29] However, inclusion of the interaction with the underlying σ backbone stabilizes the C_4H_4 molecule in a singlet state with rectangular geometry. The rectangular C_4H_4 is more stable than the square geometry by 6.2 kcal/mol. In the case of Al_4 systems, because of a smaller BLA, the triplet state with D_{4h} symmetry is found to lie far above (∼60 kcal/mol) the GS singlet. In the context of C_4H_4, Longuet-Higgins and Orgel suggested that such a system can be stabilized if the nonbonding electrons form bonding molecular orbitals with suitable low-energy d orbitals of a transition metal.

4.1. $Fe(CO)_3$ Complex. A molecular complex, $\eta^4(C_4H_4)-Fe(CO)_3$, has been realized through the formation of such bonding molecular orbitals. For the Al_4M_4 systems, we have performed the GS energy analysis on the similar systems, $\eta^4(Al_4M_4)-Fe(CO)_3$, using the same level of theory mentioned above. Both the structures are shown in Figure 4. Al_4M_4 indeed forms stable η^4 complexes with $Fe(CO)_3$.

The binding energies (defined as $E_{complex} - E_{fragments}$) in $(Al_4Li_4)-Fe(CO)_3$, $(Al_4Na_4)-Fe(CO)_3$, and $(Al_4K_4)-Fe(CO)_3$ are found to be −118.85, −122.92, and −126.28 kcal/mol, respectively. For comparison, the binding energy in $(C_4H_4)-Fe(CO)_3$ is −78.44 kcal/mol. The comparable binding energies for the all-metal sandwich complexes and the organometallic complexes suggest that Al_4M_4 is very well-stabilized in the complex, in fact, even more stabilized than C_4H_4.

To understand whether the systems change their geometries upon complexation, we compute the BLA for the complexed geometries. While the free state C_4H_4 has $\Delta R = 0.24$ Å, in the complex, $\eta^4(C_4H_4)-Fe(CO)_3$, the ΔR for the C_4H_4 ring is only 0.005 Å. Thus, C_4H_4, when complexed, is a square rather than a rectangle and, as expected from the π-only interaction, it behaves as aromatic $C_4H_4^{2-}$.

In the complexes, $(Al_4M_4)-Fe(CO)_3$, the BLAs are very small [0.028, 0.0345, and 0.041 Å in $(Al_4Li_4)Fe(CO)_3$, $(Al_4Na_4)Fe(CO)_3$, and $(Al_4K_4)Fe(CO)_3$, respectively]. Such a large decrease in ΔR clearly supports that the Al_4M_4 ligands have been converted into a six π $Al_4M_4^{2-}$ species, accounting for their substantial stability because of aromaticity.

4.2. Metal Sandwich Complex. Another well-known methodology in stabilizing an unstable molecule is to form a sandwich type of geometry, where two molecular species can share the interaction with a transition metal; cyclo-

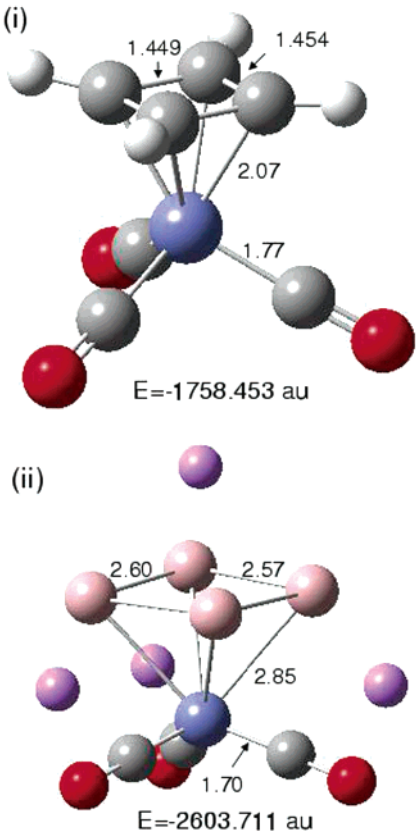

FIGURE 4. Equilibrium minimum energy geometries for (i) $\eta^4(C_4H_4)$—$Fe(CO)_3$ and (ii) $\eta^4(Al_4Li_4)$—$Fe(CO)_3$. Bond lengths are in angstroms. Ball color: red, O; violet, Fe; black, C; pink, Li; white, H; and light brown, Al.

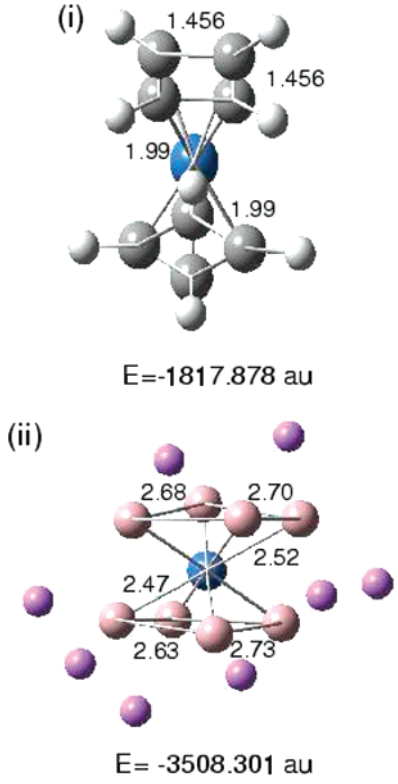

FIGURE 5. Equilibrium minimum energy geometries for (i) $(C_4H_4)_2Ni$ and (ii) $(Al_4Li_4)_2Ni$. Distances are in angstroms. Ball color: black, C; pink, Li; white, H; light brown, Al; and blue, Ni.

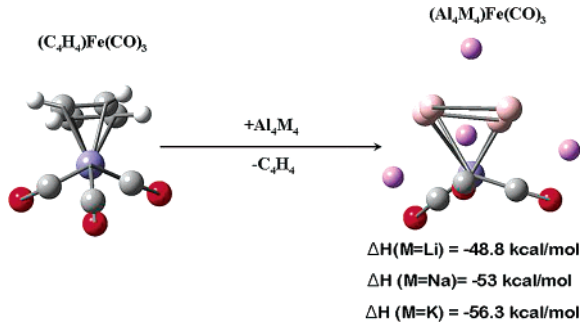

FIGURE 6. Substitution reactions in $(C_4H_4)Fe(CO)_3$ by Al_4Li_4, Al_4Na_4, and Al_4K_4 to produce $(Al_4Li_4)Fe(CO)_3$, $(Al_4Na_4)Fe(CO)_3$, and $(Al_4K_4)Fe(CO)_3$. Note that all of these substitutions are highly exothermic. Pink balls indicate the alkali metal ions.

pentadiene is stabilized in such a geometry, resulting in the ferrocene structure.[30] After performing the geometry optimization at the same level of theory discussed above, we find that the structure for $(C_4H_4)_2Ni$ is indeed a sandwich geometry, with the two C_4H_4 rings above and below the Ni atom [see (i) in Figure 5]. In this complex, the Ni atom sits symmetrically inside the cavity of the two C_4H_4 rings with a distance of 1.99 Å from each C_4H_4 ring. The two C_4H_4 molecules, however, remain staggered to each other.

Similarly, we have stabilized the Al_4M_4 clusters by introducing them in sandwiches of the type: $(Al_4M_4)_2Ni$. The geometry for the $(Al_4Li_4)_2Ni$ is shown in (ii) in Figure 5. The central Ni atom sits asymmetrically in the cavity of the two Al_4Li_4 rings. Recent theoretical studies by Mercero et al. on its aromatic analogue, Al_4^{2-}, support our claim.[31]

The binding energies for $(Al_4Li_4)_2Ni$, $(Al_4Na_4)_2Ni$, and $(Al_4K_4)_2Ni$ are 146.054, −147.12, and −103.12 kcal/mol, respectively. For C_4H_4, the same binding energy is −150.819 kcal/mol.

4.3. Substitution Reaction. Because C_4H_4 complexes are already known,[28] for the realization of all-metal complexes, we carry out calculations with substitution within conventional organometallic complexes. In Figure 6, we show the substitution reactions in $(C_4H_4)Fe(CO)_3$ by Al_4M_4 to produce $(Al_4M_4)Fe(CO)_3$. The enthalpies for the reactions are highly exothermic with $\Delta H = -48.8$, −53, and −56.3 kcal/mol for M = Li, Na, and K, respectively.

For the full-sandwich complexes, $(Al_4M_4)_2Ni$, the lowest binding energy is for $(Al_4K_4)_2Ni$ (see structures in Figure 7). This arises from the distortion in the sandwich architecture because of the presence of the bulky K^+ ions, as a result of which the average K^+ distance to the Al_4^{4-} ring is very large (3.5 Å). For $(Al_4Li_4)_2Ni$ and $(Al_4Na_4)_2Ni$, the average M^+ distance from the Al_4^{4-} ring is 3.0 Å. The binding energy for $(C_4H_4)_2Ni$ (calculated as mentioned in the previous section) is −150.819 kcal/mol, and thus, unlike the cases for (Al_4M_4)—$Fe(CO)_3$, direct substitution of C_4H_4 with Al_4M_4 will be highly endothermic for the full-sandwich complexes and thus quite unfavorable.

Instead, we consider a substitution reaction of the type: $(C_4H_4)_2Ni + Al_4M_4 = (C_4H_4)Ni(Al_4M_4) + C_4H_4$. As has

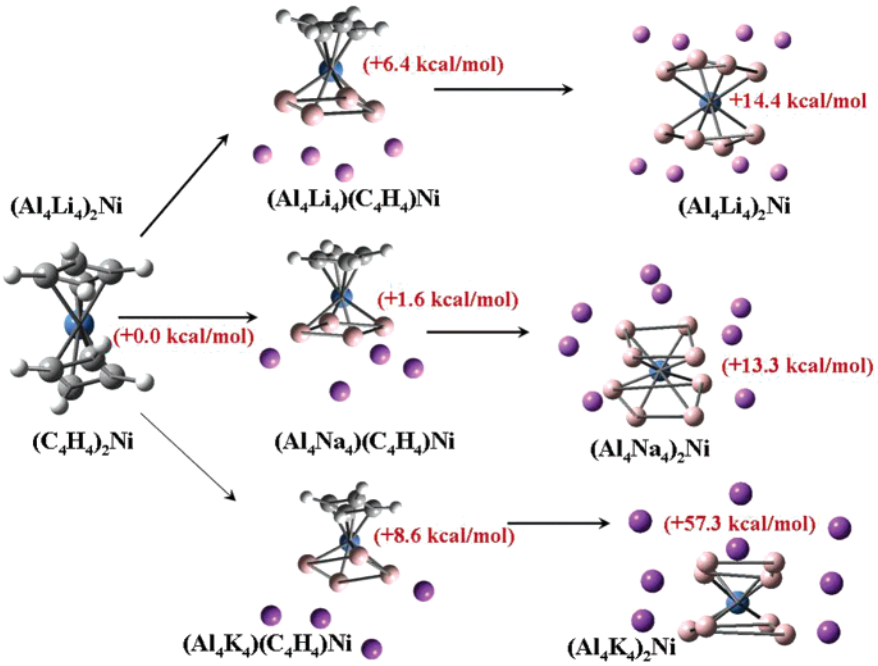

FIGURE 7. Stepwise synthesis for all-metal sandwich complexes from the organometallic complex $(C_4H_4)_2Ni$. The energy for $(C_4H_4)_2Ni$ has been scaled to zero to show the endothermic substitution reactions (the ΔE are shown in brackets). Pink balls indicate the alkali metal ions.

already been mentioned in the previous section, the Al_4M_4 (M = Li, Na, and K) binds quite strongly to the metal center. Therefore, one expects that it is possible to synthesize a hybrid organic−inorganic sandwich complex. The structures of these hybrid complexes are found to be quite stable. The heat of formation for $(C_4H_4)Ni(Al_4Li_4)$, $(C_4H_4)Ni(Al_4Na_4)$, and $(C_4H_4)Ni(Al_4K_4)$ is −153.93, −158.82, and −151.80 kcal/mol, respectively.

We rationalize the synthesis of these sandwich complexes in a three step reaction of the type: $(C_4H_4)Ni(C_4H_4)$ to $(C_4H_4)Ni(Al_4M_4)$ and finally to $(Al_4M_4)Ni(Al_4M_4)$ (as shown in Figure 7). As mentioned above, the intermediate complexes, $(C_4H_4)Ni(Al_4M_4)$, are quite stable and can thus be isolated. However, these substitution reactions are mildly endothermic. In this series, the heat of formation is the least endothermic for both $(Al_4Na_4)Ni(C_4H_4)$ and $(Al_4Na_4)_2Ni$. Therefore, we propose that $(Al_4Na_4)Ni(C_4H_4)$ and $(Al_4Na_4)_2Ni$ are the best candidates for isolation.

5. Stabilization of All-Metal Aromatic/Antiaromatic Clusters through the Formation of Superclusters

Intermolecular interactions between aromatic systems (π stacking) have been extensively studied during the past 2 decades, both experimentally and theoretically.[32,33] Detailed potential energy surface (PES) calculations for π stacks show the presence of a local minimum in the PES, which favors the formation of π stacks in aromatic molecules over the nascent molecule.[34]

In a similar context, it will be interesting to ask if the all-metal aromatic or antiaromatic molecules also form similar π-stacked dimers or form entirely different new superclusters. In fact, Al_3^- has been shown to form a stable dimer, Al_6^{2-}.[35] To address this issue, we consider $[Al_4]^{2-}$ and $[Al_4]^{4-}$ as the monomers for modeling the aromatic and antiaromatic stacked dimers and compare them with their organic analogues. Electron correlation was taken into account by using the second-order Møller−Plesset perturbation method (MP2)[36] at the 6-31+G(d,p) basis set level.

We optimized the dimer structures of C_6H_6, C_4H_4, $[Al_4]^{2-}$, and $[Al_4]^{4-}$ at the above level of theory (see Figure 8 for structures). As shown, the optimized geometry of $(C_6H_6)_2$ corresponds to the well-characterized slipped parallel π-stacked dimer (perpendicular distance, $d = 3.62$ Å). The geometry of $(C_4H_4)_2$ corresponds to a completely slipped parallel π-stacked dimer, $d = 2.96$ Å. The PESs for the systems are analyzed to understand the stability of the dimers. The energies at each configuration are determined by varying the perpendicular distance between the two monomer rings. For the $([Al_4]^{2-})_2$ and $([Al_4]^{4-})_2$ clusters, pseudo-ring centers are used to calculate the perpendicular ring−ring distances. The PESs for all of the systems are plotted in Figure 9.

The stabilization energy (ΔE) is calculated as the energy difference between the dimer and the monomer: $\Delta E = E(\text{dimer}) - 2E(\text{monomer})$. Note that this energy is corrected for the basis-set superposition error (BSSE) through the counterpoise (CP) correction scheme.[37] For the organic systems, $(C_6H_6)_2$ and $(C_4H_4)_2$, we find the stabilization energy (ΔE) to be −2.23 and −3.52 kcal/mol, respectively. The negative value for the stabilization energy corresponds to the formation of a stable dimer structure. However, for the all-metal systems, ΔE values are 89.96 and 616.98 kcal/mol for $([Al_4]^{2-})_2$ and $([Al_4]^{4-})_2$, respectively.

The apparent destabilization of the superclusters, $([Al_4]^{2-})_2$ and $([Al_4]^{4-})_2$, is due to the fact that, while $(C_6H_6)_2$/$(C_4H_4)_2$ are neutral, their Al analogues have formal nega-

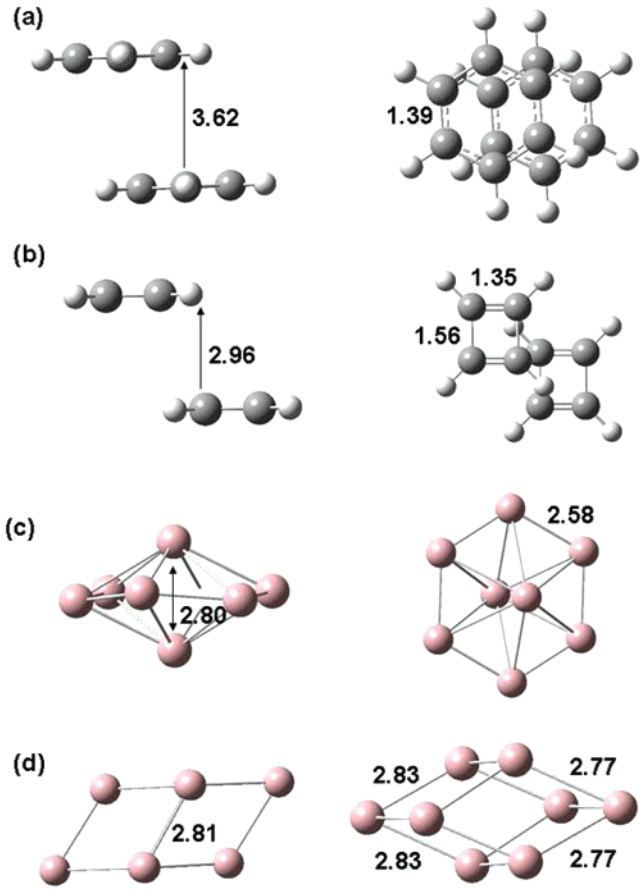

FIGURE 8. Optimized geometries of the aromatic and antiaromatic dimers (side and top views): (a) C_6H_6 stack, (b) C_4H_4 stack, (c) $[Al_4]^{2-}$ cluster, and (d) $[Al_4]^{4-}$ cluster. The bond lengths and distances are reported in angstroms. Color code: black, carbon; white, hydrogen; and pink, aluminum.

tive charges [4 and 8 formal negative charges for $([Al_4]^{2-})_2$ and $([Al_4]^{4-})_2$, respectively].

To remove the Coulombic repulsions because of large formal negative charges, we consider a dipositive metal ion, such as Ca^{2+}, as the neutralizing charge and perform geometry optimization for these clusters at the same level of theory as discussed above. The structures are shown in Figure 10. The corresponding stabilization energies (ΔE) for $([Al_4]^{2-}\ Ca^{2+})_2$ and $([Al_4]^{4-}\ (Ca^{2+})_2)_2$ are found to be -131.59 and -114.49 kcal/mol, respectively. The negative value of ΔE and the large magnitude of the same stabilization energy indicate that the superclusters are substantially stable.

6. Summary and Future Prospects

Major advances have been made in the past decade toward an atomistic understanding of the structure and properties in nanoscale systems. The concept of aromaticity and antiaromaticity have been introduced for all-metal clusters. Although there exist some obvious similarities between these systems and the organic compounds, additional care is certainly required for the correct assignment of aromatic characteristics to these systems. The need for a direct methodology to characterize the role of the σ backbone and the π electrons is becoming all the more essential, with new reports of aromaticity and antiaromaticity rapidly emerging in the literature for new molecules. A simple method to partition the distortion energies belonging to σ and π electrons applicable for a large class of systems with closely spaced σ and π electronic levels is presented in this Account.

From the point of view of applications, these Al_4M_4 clusters show a very large off-resonance third harmonic generation that is 10 000 times larger than their organic analogues. These NLO-active molecules can be stabilized through complexation to low-valent transition metals, such as Fe(0) and Ni(0). Al_4M_4 forms stable 18 electron

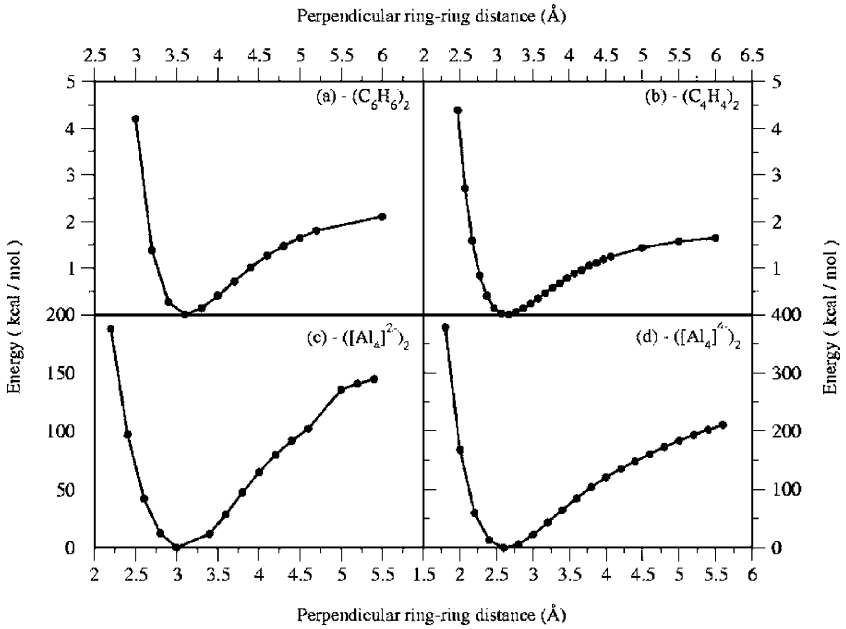

FIGURE 9. PES for the systems under study: (a) C_6H_6 stack, (b) C_4H_4 stack, (c) $([Al_4]^{2-})_2$ cluster, and (d) $([Al_4]^{4-})_2$ cluster. The perpendicular ring−ring distances are reported in angstroms, and energy is reported in kcal/mol.

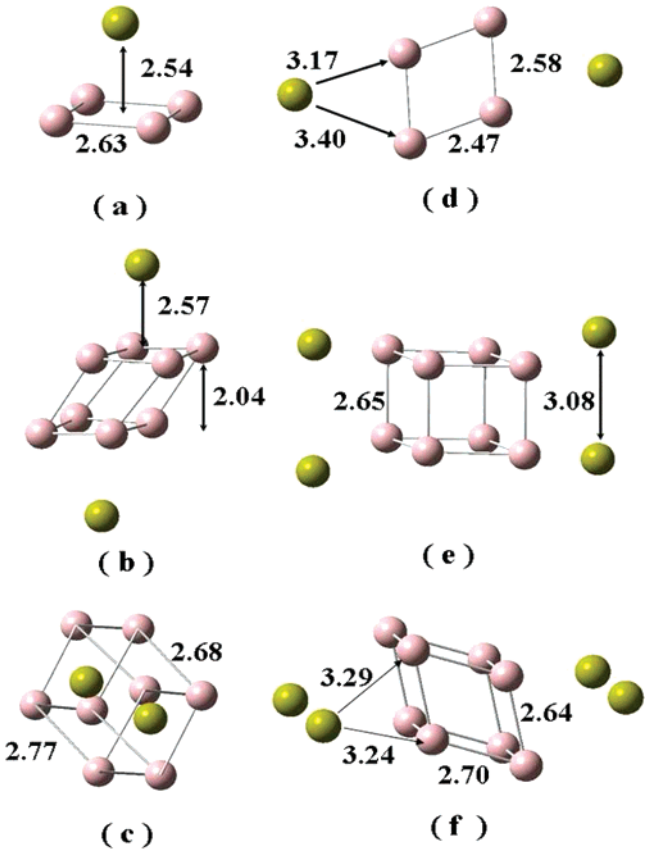

FIGURE 10. Optimized geometries of the aromatic and antiaromatic metal-chelated neutral species: (a) $([Al_4]^{2-})Ca^{2+}$, (b) $([Al_4]^{2-})_2(Ca^{2+})_2$ side view, (c) $([Al_4]^{2-})_2(Ca^{2+})_2$ top view, (d) $([Al_4]^{4-})(Ca^{2+})_2$, (e) $([Al_4]^{4-})_2(Ca^{2+})_4$ side view, and (f) $([Al_4]^{4-})(Ca^{2+})_4$ top view. The bond lengths and distances are reported in angstroms. Color code: pink, aluminum; and yellow, calcium.

half-sandwich and full-sandwich complexes, such as $(Al_4M_4)Fe(CO)_3$ and $(Al_4M_4)_2Ni$. In fact, $(Al_4M_4)Fe(CO)_3$ can be readily formed from its organic counterpart, (C_4H_4)-$Fe(CO)_3$, by the substitution reaction of Al_4M_4 by C_4H_4. Additionally, these all-metal clusters form extremely stable compact superclusters through dimerization, which are aromatic.

Future research in the area of nanoclusters would consist of hybrid systems with nonlocal and multidirectional charge distributions. A parallel between purely metallic clusters and organic molecules would certainly bridge the subject gap between physics and chemistry. New synthetic routes with advanced crystallography would help rationalize many of these possibilities. Major advances in theoretical modeling of these materials will, however, require new and rigorous frameworks that will accurately and unambiguously assign stability criteria within these systems. The ever increasing computational resources available to the quantum chemists would certainly facilitate all-electron calculations for large clusters, leading to an universal understanding of various energy-scale interactions at the nanoscale.

S.K.P. thanks DST, Government of India, for the research grants. A.D. and S.S.M. thank CSIR–India for the senior and junior research fellowships, respectively.

References

(1) (a) Ratner, M.; Ratner, D. *Nanotechnology: A Gentle Introduction to the Next Big Idea*; Prentice Hall: New York, 2002. (b) Borisenko, V. E.; Ossicini, S. *What Is What in the Nanoworld: A Handbook on Nanoscience and Nanotechnology*; Wiley-VCH: Weinheim, Germany, 2004.

(2) Zhou, B. *Nanotechnology in Catalysis*; Plenum Press: New York, 2004.

(3) Zhao, L.; Kelly, K. L.; Schatz, G. C. The Extinction Spectra of Silver Nanoparticle Arrays: Influence of Array Structure on Plasmon Resonance Wavelength and Width. *J. Phys. Chem. B* **2003**, *107*, 7343–7350.

(4) Li, X.; Kuznetsov, A.; Zhang, H-F.; Boldyrev, A. I.; Wang, L. Observation of All-Metal Aromatic Molecules. *Science* **2001**, *291*, 859–861.

(5) (a) Li, X.; Zhang, H-F.; Wang, L.-S.; Kuznetsov, A. E.; Cannon, N. A.; Boldyrev, A. I. Experimental and Theoretical Observations of Aromaticity in Heterocyclic XAl_3^- (X = Si, Ge, Sn, Pb) Systems. *Angew. Chem., Int. Ed.* **2001**, *40*, 1867–1870. (b) Chattaraj, P. K.; Roy, D. R.; Elango, M.; Subramanian, V. Chemical Reactivity Descriptor Based Aromaticity Indices Applied to Al_4^{2-} and Al_4^{4-} Systems. *J. Mol. Struct.* **2006**, *759*, 109–110.

(6) (a) Kuznetsov, A.; Boldyrev, A. I.; Li, X.; Wang, L.-S. On the Aromaticity of Square Planar Ga_4^{2-} and In_4^{2-} in Gaseous $NaGa_4^-$ and $NaIn_4^-$ Clusters. *J. Am. Chem. Soc.* **2001**, *123*, 8825–8831. (b) Alexandrova, A. N.; Boldyrev, A. I.; Zhai, H.-J.; Wang, L.-S. $Cu_3C_4^-$ A New Sandwich Molecule with Two Revolving C_2^{2-} Units. *J. Phys. Chem. A* **2005**, *109*, 562–570. (c) Datta, A.; John, N. S.; Kulkarni, G. U.; Pati, S. K. Aromaticity in Stable Tiara Nickel Thiolates: Computational and Structural Analysis. *J. Phys. Chem. A* **2005**, *109*, 11647–11649. (d) Datta, A.; Pati, S. K. Li and Be Clusters: Structure, Bonding and Odd–Even Effects in Half-Filled Systems. *Comput. Lett.***2005**, *1*, 271.

(7) Boldyrev, A. I.; Wang, L.-S. All-Metal Aromaticity and Antiaromaticity. *Chem. Rev.* **2005**, *105*, 3716–3757, and references therein.

(8) Tsipis, C. A. DFT Study of "All-Metal" Aromatic Compounds. *Coord. Chem. Rev.* **2005**, *249*, 2740–2762, and references therein.

(9) (a) Kuznetsov, A.; Birch, K.; Boldyrev, A. I.; Li, X.; Zhai, H.; Wang, L. All-Metal Antiaromatic Molecule: Rectangular Al_4^{4-} in the $Li_3Al_4^-$ Anion. *Science* **2003**, *300*, 622–625, and references therein. (b) Shetty, S.; Kar, R.; Kanhare, D. G.; Pal, S. Intercluster Reactivity of Metalloaromatic and Antiaromatic Compounds and Their Applications in Molecular Electronics: A Theoretical Investigation. *J. Phys. Chem. A* **2006**, *110*, 252–256, and references therein.

(10) Chen, Z.; Corminboeuf, C.; Heine, T.; Bohmann, J.; Schleyer, P. V. R. Do All-Metal Antiaromatic Clusters Exist? *J. Am. Chem. Soc.* **2003**, *125*, 13930–13931.

(11) Chen, Z.; Wannere, C. S.; Corminboeuf, C.; Puchta, R.; Schleyer, P. V. R. Nucleus-Independent Chemical Shifts (NICS) as an Aromaticity Criterion. *Chem. Rev.* **2005**, *105*, 3842–3888.

(12) Santos, J. C.; Andres, J.; Aizman, A.; Fuentealba, P. An Aromaticity Scale Based on the Topological Analysis of the Electron Localization Function Including σ- and π-Contributions. *J. Chem. Theory Comput.* **2005**, *1*, 83–86.

(13) Lin, Y.-C.; Juselius, J.; Sundholm, D.; Gauss, J. Magnetically Induced Current Densities in Al_4^{2-} and Al_4^{4-} Species Studied at the Coupled-Cluster Level. *J. Chem. Phys.* **2005**, *122*, 214308.

(14) Ritter, S. Deciphering Metal Aromaticity. *Chem. Eng. News* **2003**, *81*, 23.

(15) Datta, A.; Pati, S. K. Rationalization of the $\pi-\sigma$ (Anti)aromaticity in All Metal Molecular Clusters. *J. Chem. Theory Comput.* **2005**, *1*, 824–826.

(16) Datta, A.; Pati, S. K. Charge-Transfer Induced Large Nonlinear Optical Properties of Small Al Clusters: Al_4M_4 (M = Li, Na, and K). *J. Phys. Chem. A* **2004**, *108*, 9527–9530.

(17) Datta, A. Pati, S. K. Stable Transition Metal Complexes of an All-Metal Antiaromatic Molecule (Al_4Li_4): Role of Complexations. *J. Am. Chem. Soc.* **2005**, *127*, 3496–3500.

(18) Datta, A.; Pati, S. K. New Examples of Metalloaromatic Al-Clusters: $(Al_4M_4)Fe(CO)_3$ (M = Li, Na and K) and $(Al_4M_4)_2Ni$: Rationalization for Possible Synthesis. *Chem. Commun.* **2005**, 5032.

(19) Mallojosyula, S. S.; Datta, A.; Pati, S. K. Aromatic Superclusters from All-Metal Aromatic and Antiaromatic Monomers, $[Al_4]^{2-}$ and $[Al_4]^{4-}$. *J. Phys. Chem. B* **2006**, *110*, 20098–20101.

(20) Jug, K.; Hiberty, P. C.; Shaik, S. $\sigma-\pi$ Energy Separation in Modern Electronic Theory for Ground States of Conjugated Systems. *Chem. Rev.* **2001**, *101*, 1477–1500, and references therein.

(21) Shaik, S.; Shurki, A.; Danovich, D.; Hiberty, P. C. A Different Story of π-Delocalization—The Distortivity of π-Electrons and Its Chemical Manifestations. *Chem. Rev.* **2001**, *101*, 1501–1540, and references therein.

(22) Johnson, B.; Chen, W.; et al. *Gaussian 03*, Revision B.05; Gaussian, Inc.: Pittsburgh, PA, 2003.
(23) (a) Prasad, P. N.; Williams, D. J. *Introduction to Nonlinear Optical Effects in Moleculesand Polymers*; Wiley: New York, 1991. (b) Datta, A. Pati, S. K. Dipolar Interactions and Hydrogen Bonding in Supramolecular Aggregates: Understanding Cooperative Phenomena for 1st Hyperpolarizability. *Chem. Soc. Rev.* **2006**, *35*, 1305−1323 and references therein.
(24) (a) Marks, T. J.; Ratner, M. A. Design, Synthesis, and Properties of Molecule-Based Assemblies with Large Second-Order Optical Nonlinearities. *Angew. Chem., Int. Ed. Engl.* **1995**, *34*, 155−173, and references therein. (b) Datta, A.; Pati, S. K. Dipole Orientation Effects on Nonlinear Optical Properties of Organic Molecular Aggregates. *J. Chem. Phys.* **2003**, *118*, 8420.
(25) (a) Puspendu K. Das, Chemical Applications of Hyper-Rayleigh Scattering in Solution. *J. Phys. Chem. B* **2006**, *110*, 7621−7630, and references therein. (b) Datta, A.; Pati, S. K. Nonlinear Optical Properties in Calix[*n*]arenes: Orientation Effects of Monomers. *Chem.—Eur. J.* **2005**, *11*, 4961.
(26) Zerner, M. C.; Loew, G. H.; Kirchner, R. F.; Mueller-Westerhoff, U. T. An Intermediate Neglect of Differential Overlap Technique for Spectroscopy of Transition-Metal Complexes. Ferrocene. *J. Am. Chem. Soc.* **1980**, *102*, 589−599, and references therein.
(27) Beljonne, D.; Cornil, J.; Friend, R. H.; Janssen, R. A. J.; Bredas, J. L. Influence of Chain Length and Derivatization on the Lowest Singlet and Triplet States and Intersystem Crossing in Oligothiophenes. *J. Am. Chem. Soc.* **1996**, *118*, 6453−6461.
(28) Collman, J. P.; Hegedus, L. S.; Norton, J. R.; Finke, R. G. *Principles and Applications of Organotransition Metal Chemistry*; University Science Books: Oxford, U.K., 1987.
(29) Salem, L. *The Molecular Orbital Theory of Conjugated Systems*; Benjamin, Inc.: New York, 1966.
(30) Wilkinson, G.; Rosenblum, M.; Whiting, M. C.; Woodward, R. B. The Structure of Iron Bis-cyclopentadienyl, *J. Am. Chem. Soc.* **1952**, *74*, 2125−2126.
(31) Mercero, J. M.; Formoso, E. Matxain, J. M.; Eriksson, L. A.; Ugalde, J. M. Sandwich Complexes Based on the "All-Metal" Al_4^{2-} Aromatic Ring. *Chem.—Eur. J.* **2006**, *12*, 4496, and references therein.
(32) Kwang S. Kim, Tarakeshwar, P. Lee, J. Y. Molecular Clusters of π-Systems: Theoretical Studies of Structures, Spectra, and Origin of Interaction Energies. *Chem. Rev.* **2000**, *100*, 4145−4186, and references therein.
(33) Muller-Dethlefs, K.; Hobza, P. Noncovalent Interactions: A Challenge for Experiment and Theory. *Chem. Rev.* **2000**, *100*, 143−168, and references therein.
(34) Tsuzuki, S.; Honda, K.; Uchimaru, T.; Mikami, M.; Tanabe, K. Origin of Attraction and Directionality of the π/π Interaction: Model Chemistry Calculations of Benzene Dimer Interaction. *J. Am. Chem. Soc.* **2002**, *124*, 104−112.
(35) Kuznetsov, A. E.; Boldyrev, A. I.; Zhai, H. J.; Li, X.; Wang, L. S. Al_6^{2-}—Fusion of Two Aromatic Al_3^- Units. A Combined Photoelectron Spectroscopy and *ab Initio* Study of $M^+Al_6^{2-}$] (M = Li, Na, K, Cu, and Au). *J. Am. Chem. Soc.* **2002**, *124*, 11791−11801.
(36) Møller, C.; Plesset, M. S. Note on an Approximation Treatment for Many-Electron Systems, *Phys. Rev.* **1934**, *46*, 618.
(37) Salvador, P.; Duran, M. The Effect of Counterpoise Correction and Relaxation Energy Term to the Internal Rotation Barriers: Application to the $BF_3\cdots NH_3$ and $C_2H_4\cdots SO_2$ Dimers. *J. Chem. Phys.* **1999**, *111*, 4460, and references therein.

AR0682738